Experimental Measurements of Hydrodynamic Radial Forces and Stiffness Matrices for a Centrifugal Pump-Impeller

Dimitri S. Chamieh[1]
Assoc. Mem. ASME

Allan J. Acosta
Fellow ASME

Christopher E. Brennen
Mem. ASME

Thomas K. Caughey

California Institute of Technology,
Pasadena, CA 91125

The present work is an experimental investigation of the possible forces of fluid dynamic origin that can act on a turbomachine rotor particularly when it is situated off its normal center position. An experimental facility, the Rotor Force Test Facility, has been designed and constructed in order to measure these kinds of forces acting on a centrifugal pump impeller when the latter is made to whirl in a slightly eccentric circular orbit. The scope of the present experimental work consists of measuring quasi-steady forces on the impeller as it whirls slowly about the axis of the pump rotation. These forces are due to interaction between the impeller and volute; they are decomposed into force components relative to the geometric center of the volute and to those proportional to displacement from this center. These latter are interpreted as stiffness matrices. Such matrices were obtained for two different volutes and both were found to be the sum of a diagonal and a skew-symmetric matrix. It can be shown that a stiffness matrix of this type can lead to dynamic instability of impeller shaft system in certain circumstances. This new experimental finding may explain some operational problems of "high-speed" hydraulic machinery. Comparison is made with various existing theoretical and experimental results.

Introduction

It has become evident in the past few years that hydrodynamic effects due to the presence of the rotor itself, in addition to the seals and bearings, may also cause rotor whirl. Such problems have been experienced not only in steam turbines (Pollman, et al. [13]) but also in large compressors (Thompson [15]) and in high speed pumps (Ek [8]). Here the flow through the turbomachine rotor and its surroundings induces a fluid dynamic force on the rotor shaft that may be a cause for rotor whirl. We have proposed in the past [2] an experiment with the capabilities of measuring impeller forces for any whirling rotor. This paper reports preliminary data from the first stage experiments in which the shaft is orbited at a very low frequency.

Steady State-Radial Force

A major problem centrifugal pump designers must cope with is the radial load on the impeller caused by the nonuniformity of the static pressures and velocities within the volute, particularly at off-design conditions. The reason for this nonuniformity is the mismatching of impeller and volute leading to changes of flow rate and total head around the impeller outlet. The literature dealing with this force is quite extensive. Many of the earlier references are based on the semi-empirical relation quoted by Stepanoff [14]:

$$F_0 = K\Delta P_t d_2 w_2 \tag{1}$$

where K is a parameter depending on the type of volute casing used and on flow rate (see also [14]). Other experimental works followed in the same spirit, namely, those of Agostinelli, et al. [1], Iversen, et al. [10], and Domm and Hergt [7]. Among the theoretical papers on the subject are the source vortex method of Domm and Hergt [7] and Colding-Jorgensen [6] and the actuator disk model of Chamieh and Acosta [3, 4]. Most of these previous works will be compared to the actual experimental findings.

Hydrodynamic Stiffness Matrix

Colding-Jorgensen [6] first introduced the concept of hydrodynamic stiffness matrices in order to express the sensitivity of the radial forces to the position of the impeller. He solved a theoretical model based on the source-vortex model of an impeller inside a logarithmic spiral volute. Here, even at design flow we may still expect a hydraulic force to be exerted on the impeller caused by the distortion of the streamlines within the volute due to displacement of the impeller from the geometric center of the volute.

The displacement of the impeller from the geometric center of the volute can arise from many sources, e.g., manufac-

[1] Presently, Byron Jackson Pump Division, Borg Warner Industrial Products, Inc., Long Beach, CA, 90802.

Contributed by the Fluids Engineering Division for publication in the JOURNAL OF FLUIDS ENGINEERING. Manuscript received by the Fluids Engineering Division, April 2, 1984.

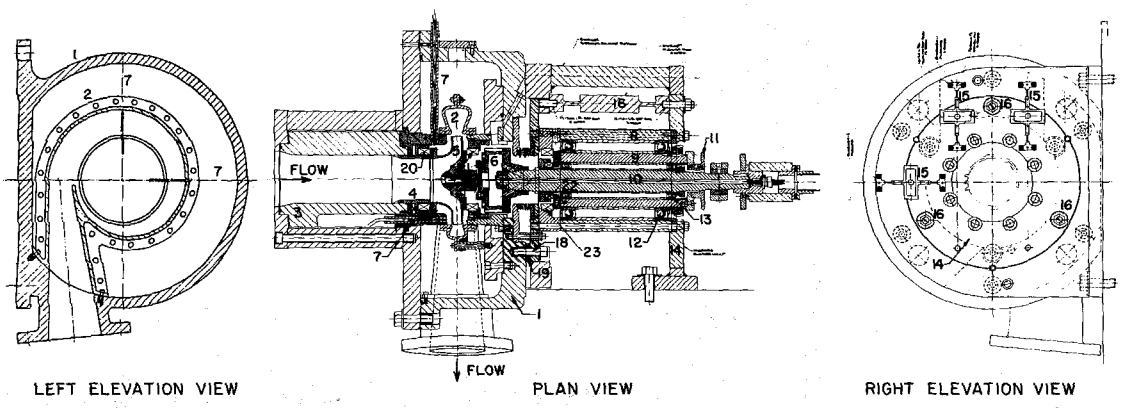

Fig. 1 Machine drawing of the impeller, volute, internal balance, eccentric drive, pump housing and external balance assembly of the Rotor Force Test Facility. Pump housing (1); volute (2); inlet connection (3); inlet bell (4); impeller (5); internal balance (6); proximity probes (7); eccentric drive mechanism: outer bearing carrier (8), inner bearing carrier (9), main shaft (10), orbiting motion sprocket (11) and bearings (12, 13); external balance: flexure face (14), flexure elements (15, not shown in the plan view) and axial flexures (16); bellows (17); bolts linking floating system and ground (18); spacers (19); impeller front face seals (20) and back face seals (21); eccentric drive inner face seals (22) and outer face seals (23). Note: The system is shown in its caged position. Removal of bolts (18) and spacers (19) will make unit float (see also text).

turing tolerances, weight, vibrational disturbances, unbalanced forces or blade cut-water forces etc. In this situation the hydraulic forces caused by the relative displacement of the impeller and volute can be compared in principle to spring forces. In the radial plane of the impeller, this force vector can be linked to the displacement vector (measured from the geometric center of the volute) by a 2 × 2 stiffness matrix. A more mathematical definition of this stiffness matrix will be given in the section under "Data Reduction."

Documentation of hydrodynamic stiffness forces and matrices is exceedingly sparse. For centrifugal pumps, for example, only very limited experimentation by Domm and Hergt [7] and Hergt and Krieger [9] can be found in the literature. Domm and Hergt measured forces on an impeller for two equal eccentricities (but different angular positions) for various flow rates. Their results were not interpreted using the concepts of hydrodynamic stiffness matrices. Hergt and Krieger measured forces on an impeller for three different flow rates but for various eccentricities and angular positions. One of their conclusions is that the forces seemed to be proportional to the eccentricity for the three flow rates tested but there was still no attempt to deduce stiffness matrices. A similar experiment was conducted by Ohashi and Shoji, et al. [12]. Their test impeller was installed in a large vaneless diffuser with the result that the stiffness matrix was small and could not be detected. Besides Colding-Jorgensen [6], Chamieh [4, 5] calculated hydrodynamic stiffness matrices using very simple impeller flow models. We believe this paper is the first to report on the measurement of such matrices.

Rotor Force Test Facility

The facility was described in detail in earlier references [2, 5]. We will merely repeat that the objective of the facility is to impose known orbiting motions of radian frequency ω on the basic rotary motion of a number of typical centrifugal pump impellers (radian frequency, Ω, shaft speed, N). This paper deals only with results obtained for $\omega/\Omega \ll 1$, that is to say a quasi-static offset. The facility is shown in the machine drawing in Fig. 1. Further details can be found in [5].

A five-bladed Byron Jackson centrifugal pump designated Impeller X with an outer diameter of 162 mm and a discharge angle of 25 deg, was used for all the present measurements. A machine drawing as well as photographs can be found in [5]. This impeller was cast in bronze and has a specific speed of 0.57. A well-matched trapezoidal cross-section fiberglass

Nomenclature

A_2 = impeller discharge area = $\pi d_2 b_2$
b_2 = impeller outlet width
C_p = pressure coefficient = $(p - p_{td})/\frac{1}{2}\rho U_2^2$
d_2 = impeller outlet diameter
$\mathbf{e}$ = vectorial deflection of the external balance
$\mathbf{F}$ = impeller total force vector; components F_X and F_Y
F_N = normalizing force = $\rho U_2^2 A_2/2$
$\mathbf{F}_0$ = radial force vector; magnitude F_0 and components F_{0X} and F_{0Y}
$\mathbf{F}_\omega$ = fundamental harmonic component of $\mathbf{F}$
K = Stepanoff's parameter as defined in [14]
$[K]$ = hydrodynamic force matrix; components K_{ij} with $i, j = X, Y$
$[KP]$ = static pressure hydrodynamic force matrix; components KP_{ij} with $i, j = X, Y$
$[K_S]$ = stiffness matrix of the extenal balance system
N = main shaft speed (rpm)
p = static pressure
p_{td} = downstream total pressure
ΔP_t = total pressure rise across the pump
Q = volume flow rate
r_2 = impeller outlet radius
U_2 = impeller tip speed
w_2 = impeller outlet width including the shrouds
X, Y = axes of volute; also impeller center position within the volute axes
δ = instantaneous impeller center position with respect to the center of whirl
δ_V = distance between the volute center and the center of whirl
δ_ω = fundamental harmonic component of δ
ϵ = eccentricity vector
θ = angular position measured from the tongue
ρ = density of water
Φ = pump flow coefficient = $Q/A_2 U_2$
Ψ = pump total head coefficient = $\Delta P_t/\rho U_2^2$
ω = radian frequency of whirl motion
Ω = radian frequency of impeller rotation

Superscript

= dimensionless quantity

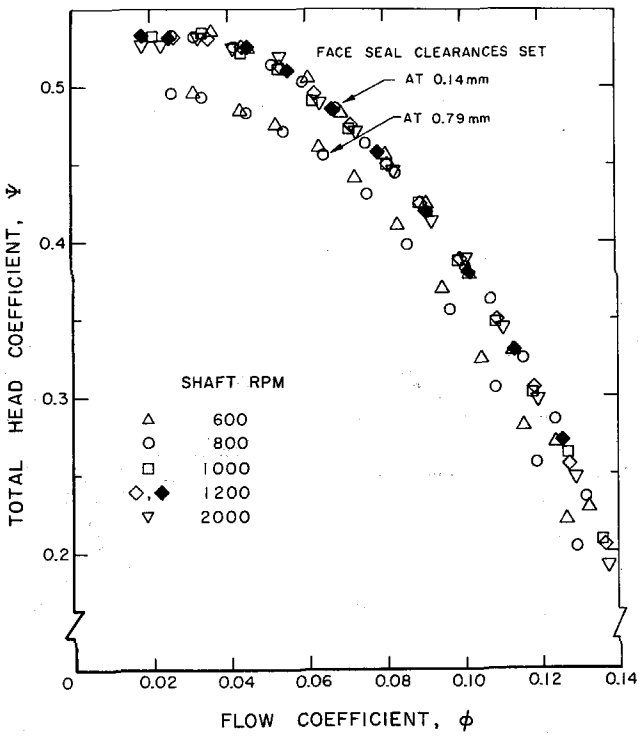

Fig. 2 Performance characteristics of Impeller *X* inside Volute *A* for the front and back face seal clearances of 0.14 and 0.79 mm. Open and closed symbols represent data for $\omega > 0$ and $\omega < 0$ respectively. (Uncertainty in $\Phi = \pm 0.0025$, in $\Psi = \pm 0.01$).

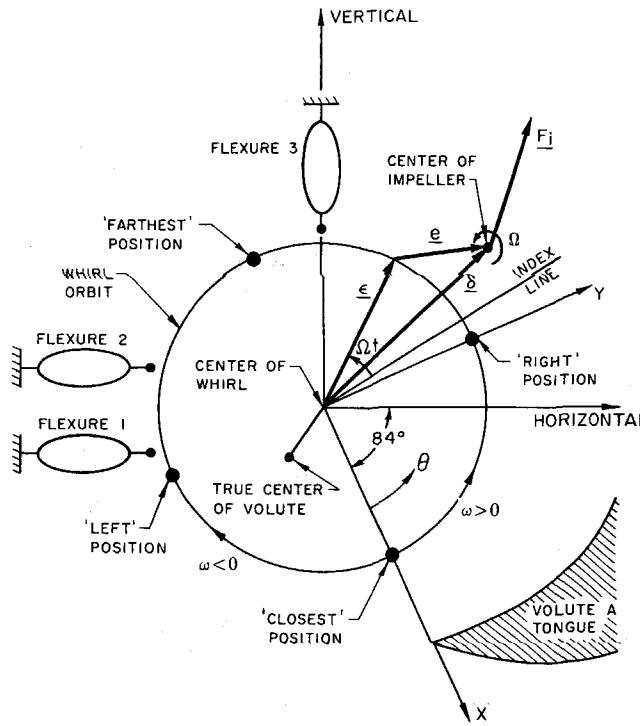

Fig. 3 Schematic of forces and locations within the impeller-volute system as seen from the inlet

volute (Volute *A*) was designed to be used with Impeller *X*. The ratio of the base circle diameter to impeller diameter is 1.13, and the area at the cutwater is 20.75 cm^2 [5]. A deliberately mismatched circular volute (Volute *B*) with a 5.42 cm constant diameter circular cross section [5] was also fabricated.

During the measurements, radial face seals on both sides of the impeller were backed off to prevent interference with the force measurements. These were selected in preference to the usual radial wear rings because the latter would interfere with the measurement of radial forces. Two sets of clearances were investigated with the radial face seals. One was considered a normal clearance in which both face seals are backed 0.14 mm from Impeller *X*. In this configuration, the inlet leakage was then estimated to be around two percent of the design flow rate. The other clearance is a deliberately large maximum clearance of 0.79 mm where inlet leakage losses are about 12 percent of the design flow rate. No experiments were made with the seals in contact. Figure 2 presents the performance characteristic of Impeller *X* for volute *A* for the two face seal clearances and for $\omega = \pm 0.314$ rad/sec.

The force balance, consisting of three strain-gauged aluminum load cells (see Fig. 1), was used with the entire impeller-eccentric drive system floating on soft spring supports attached to the ceiling. Three stainless steel axial flexures parallel with the shaft maintained the alignment in this configuration. A small d-c motor was also mounted on the floating assembly to produce a shaft orbit speed of 3 rpm. The purpose of this was to allow continuous sampling of the forces at all locations of the shaft around a circular orbit with a radius of 1.26 mm. By comparison with the forces at certain fixed locations as well as by imposing a reverse orbiting speed of 3 rpm it was determined that the dynamic effects of this 3 rpm orbit speed were negligible.

Two of the strain-gauged load cells were mounted horizontally (Fig. 1, the right elevation view) for measurement of horizontal force and torque; the other measures the vertical force. Calibrations were performed by known forces applied by systems of wires, pulleys and weights. The linearity of the calibrations was within one percent over the entire range of calibration (−20 to +20 kgf) and the interactions were less than one percent.

Signal processing was accomplished by means of an eight channel digital signal processor which was phase locked to an optical encoder attached to the shaft of the 3 rpm motor. In this way each of the eight channels of data (three load cell signals plus pressure transducers, flow rates, etc.) are sampled at 32 equally spaced positions of each rotation of the eccentricity. Furthermore this sampling was continued for 15 or more rotations in order to obtain averages of the forces for each of the 32 geometric positions.

The flexure signals were also recorded on magnetic tape and processed through a digital spectrum analyzer to investigate their content. The major peak was observed at the 3 rpm whirl frequency. Much smaller peaks also occurred at higher harmonics of this whirl frequency. The largest observed magnitude of the second harmonic was always less than ten percent of the fundamental indicating that the impeller forces at the small eccentricity employed vary quite sinusoidally around the circular eccentric orbit and that this variation can be accurately represented by a stiffness matrix.

Finally, linearity of the stiffness matrix with respect to the imposed eccentricity has been assumed in view of the previously discussed experimental data of Hergt and Krieger [9].

Data Reduction

The geometry and notation of the impeller shaft location, external balance load cells and volute position are shown in Fig. 3 (viewed from the pump inlet). The center of the volute and the center of whirl are made to coincide through proper adjustment of the spring assembly such that δ_V is minimized; ideally δ_V should be zero before any test run. The flexure system, though quite stiff, has some deflections due to the hydrodynamic forces on the impeller: This deflection **e** is

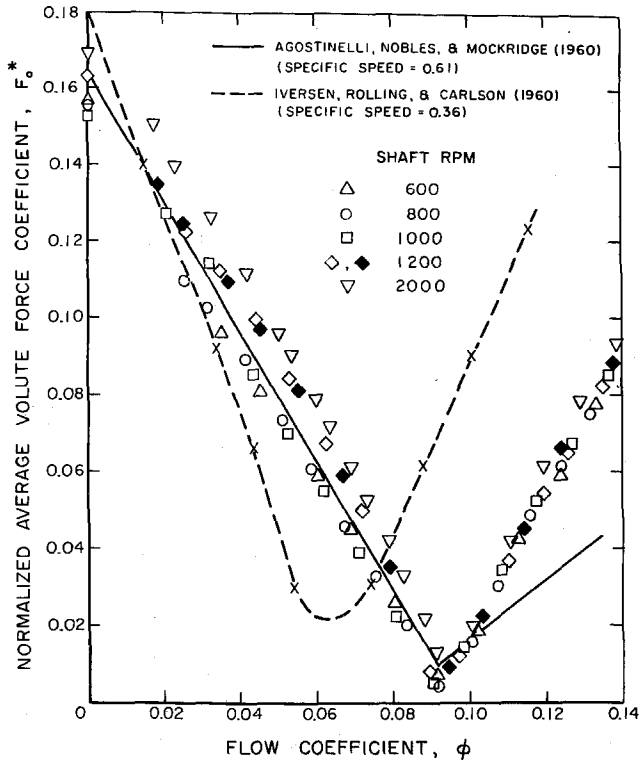

Fig. 4 Normalized average volute force for Impeller *X*, Volute *A* and face seal clearances of 0.14 mm. Open and closed symbols represent data for $\omega > 0$ and $\omega < 0$, respectively. Comparison is made with Iversen, et al. [10], bearing reactions and Agostinelli, et al. [1], experimental data. (Uncertainty in $\Phi = \pm 0.0025$, in $F_0^* = \pm 0.004$).

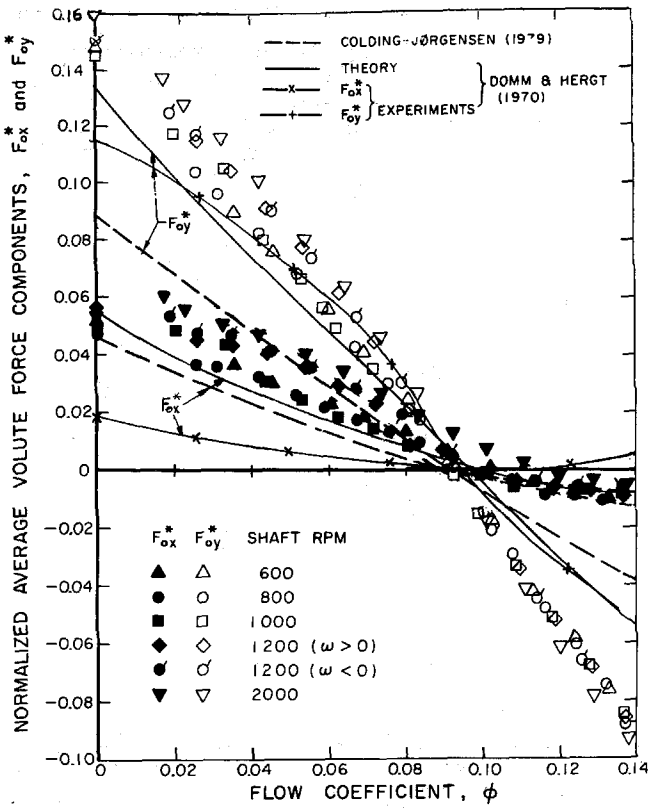

Fig. 5 Normalized average volute force components of Fig. 4 are shown along with the works of Domm and Hergt [7] and Colding-Jorgensen [6] having volute angles of 86.3° and 86°, respectively. Impeller *X*, Volute *A* and face seal clearances of 0.14 mm. (Uncertainty in $\Phi = \pm 0.0025$, in $F_0^* = \pm 0.004$).

monitored by the external balance elements. One consequence of this is that the actual position of the shaft center is a combination of the 1.26 mm eccentricity plus the deflection of the flexure system. All of the data on impeller forces were corrected for this effect. If ϵ is the instantaneous shaft center position due to the imposed eccentricity of 1.26 mm and $[K_S]$ is the stiffness matrix of the flexure system (measured by loading under conditions of no motion), then the actual instantaneous position of the shaft (see Fig. 3) is

$$\delta = \epsilon + \mathbf{e};\ \mathbf{e} = [K_S]^{-1}\mathbf{F} \tag{2}$$

where $\mathbf{F}$ is the instantaneous force acting on the rotor (and therefore on the floating assembly) for a particular test run due to the Ω and ω motions. Tare forces were found to be negligible so that, with proper zeroing of the balance, the forces, $\mathbf{F}$, are entirely hydrodynamic (see the no-impeller results in Fig. 10 for this confirmation).

Fourier decomposition of the data yields the average hydrodynamic force or radial force $\mathbf{F}_0$ associated with the mean position of the shaft center and the first harmonic, $\mathbf{F}_\omega$, associated with the first harmonic of δ, δ_ω. The hydrodynamic force matrix or stiffness matrix, $[K]$ is then defined as

$$\mathbf{F}_\omega = [K]\delta_\omega \tag{3}$$

where δ_ω is the fundamental of $\{\epsilon + [K_S]^{-1}\mathbf{F}\}$ and therefore $[K]$ can be calculated since ϵ, $[K_S]^{-1}$ and $\mathbf{F}_\omega$ are all known. In the present experiments the correction $[K_S]^{-1}\mathbf{F}_\omega$ could be as large as ten percent of δ_ω.

The forces were then nondimensionalized by the factor F_N as defined in the Nomenclature while the force matrices are nondimensionalized by F_N/r_2.

Average Volute Forces: Results and Discussion

The reduced data for the averaged dimensionless volute forces acting on Impeller *X* due to Volutes *A* and *B* are

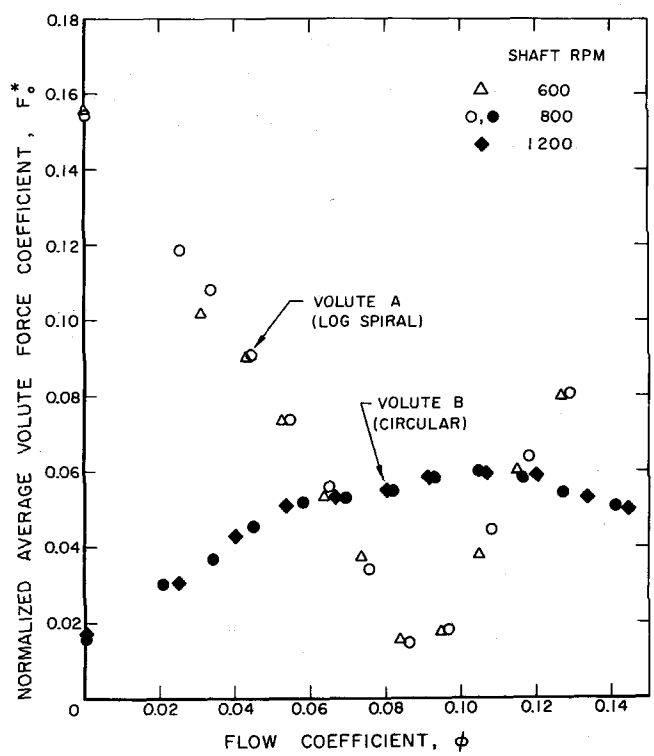

Fig. 6 Normalized average volute force for Impeller *X* and face seal clearances of 0.79 mm. Open and closed symbols represent data for Volutes *A* and *B*, respectively. (Uncertainty in $\Phi = \pm 0.0025$, in $F_0^* = \pm 0.004$).

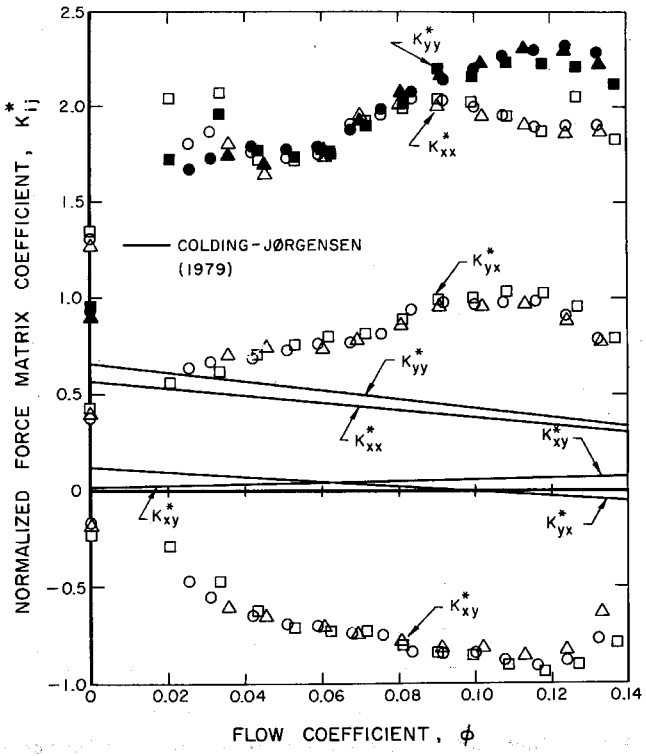

Fig. 7 Normalized force matrix coefficients as defined in text for Impeller X, Volute A and face seal clearances of 0.14 mm. Shaft speed = 600 rpm: △, ▲; 800 rpm: ○, ●; 1000 rpm: □, ■. Values of K^*_{XX}, K^*_{XY} and K^*_{YX} are represented by open symbols; values of K^*_{YY} by closed symbols. Comparison is made with Colding-Jorgensen's [6] theoretical stiffness matrix calculations with a volute angle of 86°. (Uncertainty in $\Phi = \pm 0.0025$, in $K^*_{ij} = \pm 0.05$).

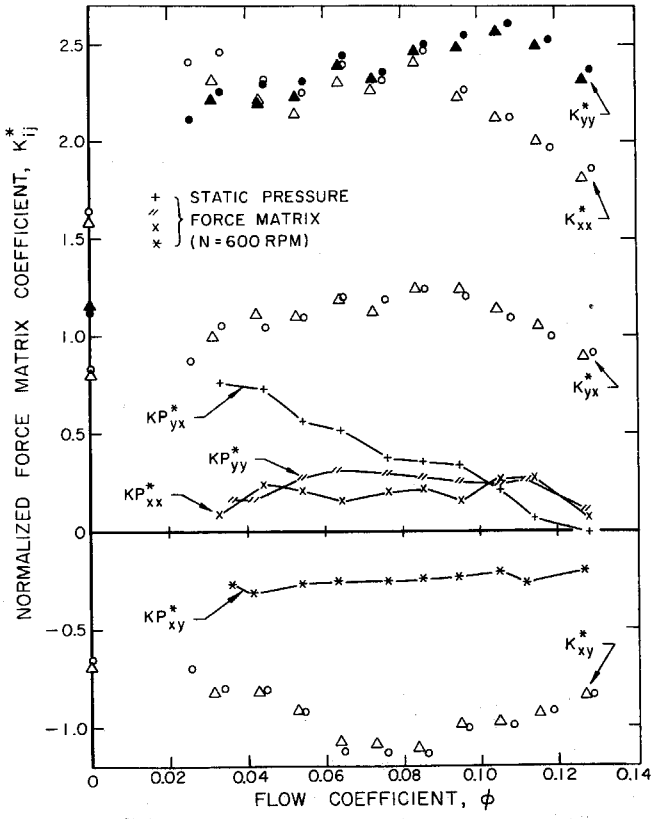

Fig. 8 Normalized force matrix coefficients as defined in text for Impeller X, Volute A and face seal clearances of 0.79 mm. Shaft speed = 600 rpm: △, ▲; 800 rpm: ○, ●. Values of K^*_{XX}, K^*_{XY} and K^*_{YX} are represented by open symbols; values of K^*_{YY} by closed symbols. The normalized static pressure force matrix for a shaft speed of 600 rpm is shown by the symbols +, ||, × and ∗. (Uncertainty in $\Phi = \pm 0.0025$, in $K^*_{ij} = \pm 0.05$).

presented in Figs. 4–6. The plots include the magnitude and individual components of the forces. The data for the "well-matched" volute (A) at a face seal clearance of 0.14 mm is shown in Fig. 4. Here F^*_0 is plotted versus flow coefficient Φ at various speeds. Some results for both a forward 3 rpm sampling orbit speed ($\omega > 0$) and a reverse orbit speed of 3 rpm ($\omega < 0$) are shown to confirm that this orbit speed had little effect on the results. The nondimensionalized force data for different shaft speeds (500 up to 2000 rpm) is in substantial agreement though there would appear to be a slight increase in the magnitude of the force coefficient at low flow coefficients when rotor speed was increased. It seems likely that this is a Reynolds number effect. From a practical viewpoint, it is clear that the Impeller X and Volute A are well matched at their design flow coefficient of 0.092 since the force on the impeller is virtually zero at this operating point. Values of F^*_0 at shutoff range from 0.155 to 0.17 which is 10–20 percent higher than the calculated value suggested by Stepanoff [14].

Also shown in Fig. 4 are the experimental results of Agostinelli, Nobles, and Mockridge [1] and Iversen, Rolling, and Carlson [10] for pumps with specific speeds of 0.61 and 0.36, respectively. The former are in close agreement with the present results since the specific speed of the present Impeller X/Volute A combination is 0.57. The results of Iversen, et al. for a lower specific speed also appear consistent with the present results. For clarity, another set of experimental results by Domm and Hergt [7] is presented in Fig. 5. These results for a volute having an angle of 86.3 deg appear to be in agreement with the present results shown in Fig. 4.

Figure 5 also presents the dimensionless force components of the average volute force. Note the direction of the total force vector is virtually independent of flow coefficient; it is almost perpendicular to the radius to the cutwater. Included in the plot are the theoretical results of Domm and Hergt [7] and Colding-Jorgensen [6] for volutes with spiral angles of about 86 deg. These theories are based on the impeller being modeled by a source-vortex at its centerline and by assuming potential flow throughout the pump stage. Volute A has a similar angle when projected on the radial plane of the impeller. However Volute A is fully three-dimensional and the equivalent spiral angle obtained by unwrapping its area would be about 82 deg. Under these assumptions the data of Colding-Jorgensen appears more consistent with the experiments than what is actually shown in Fig. 5. Unfortunately we cannot initiate a similar "correction" with the results of Domm and Hergt as the theoretical example of reference [7] featured only a volute angle of 86.3 deg.

We have also investigated the effects of an increase in the face seal clearances and a volute change on the average volute force. Figure 6 shows data for Volutes A and B for the maximum front and back face seal clearances of 0.79 mm. The magnitudes, directions (and therefore also Cartesian components) of the average volute force for Volute A exhibited almost no change for the two face seal clearances at least for the two rotor speeds tested (600 and 800 rpm cf. Fig. 4). This observation is somewhat surprising because the total head changed significantly.

Different results were found for the circular Volute (B). The force is almost constant above $\Phi = 0.07$. Below this flow rate the force coefficient decreases to a shutoff value of about 0.015. Finally, we should point out that the two speeds of 800 and 1200 rpm tested with volute B seemed to be in general agreement with respect to the normalization process.

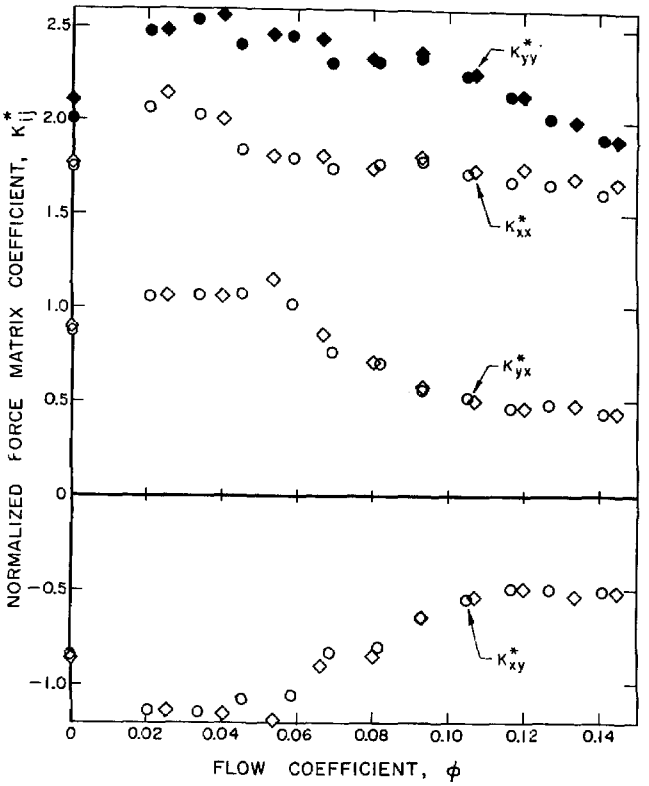

Fig. 9 Normalized force matrix coefficients as defined in text for Impeller *X*, Volute *B* and face seal clearances of 0.79 mm. Shaft speed = 800 rpm: ○, ●; 1200 rpm: ◇, ◆. Values of K^*_{XX}, K^*_{XY}, and K^*_{YX} are represented by open symbols; values of K^*_{YY} by closed symbols. (Uncertainty in $\Phi = \pm 0.0025$, in $K^*_{ij} = \pm 0.05$).

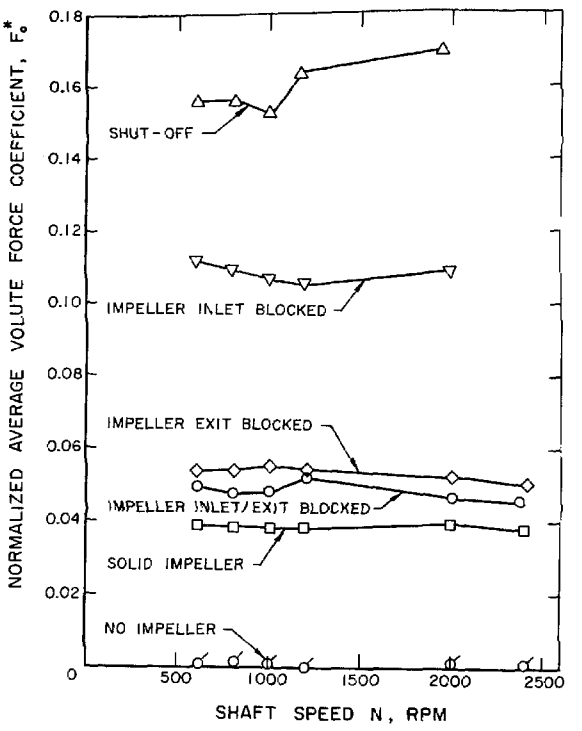

Fig. 10 Normalized average volute force is shown as a function of shaft speed for various auxiliary experiments conducted for Impeller *X*, Volute *A* and face seal clearances of 0.14 mm. (Uncertainty in $N = \pm 5$ rpm, in $F^*_\theta = \pm 0.004$).

Hydrodynamic Force Matrices

Nondimensional hydrodynamic force matrix coefficients, K^*_{ij}, are presented in Figs. 7–9. These contain all the information on how the forces presented in Figs. 4–6 vary as the position of the impeller center changes when the change is within the linear regime. Figure 7 presents data for Volute *A*, for face seal clearances of 0.14 mm, for various flow rates and for rotor speeds of $N = 600$, 800 and 1000 rpm. We observe that the variation with N is consistent with that anticipated by the nondimensionalization and that the components vary only modestly with flow coefficient, Φ, for values above about 0.03. Finally, all of the measured K^*_{ij} show a tendency to drop as we approach shutoff but they do not vanish there.

The theoretical results of Colding-Jorgensen [6] based on the source/vortex model of the impeller and depicted in Fig. 7 exhibit substantial disagreement with the measurements. The diagonal components K^*_{XX} and K^*_{YY} are about one third of those of the present experiments. The off-diagonal or "cross-coupling" terms also differ from the present values and the calculated values of K^*_{YX} exhibit a change in sign unlike its experimental counterpart.

It is worthwhile to examine closely the structure of the $[K^*]$ matrix before presenting the remaining force matrix data. In fact the hydrodynamic force matrix of Fig. 7 implies that the fluid forces tend to excite a whirl motion of the impeller. This force matrix can be presented approximately in the form

$$[K^*] = \begin{bmatrix} 2.0 & -0.9 \\ 0.9 & 2.0 \end{bmatrix} \tag{4}$$

over the range of $0.04 < \Phi < 0.14$. It is therefore a combination of a diagonal and a skew-symmetric matrix. The former will simply reduce the structural stiffness matrix and in many cases this hydrodynamic effect will be small. The skew-symmetric or cross-coupling terms are much more important. The signs of the off-diagonal terms imply that the force component tangential to the whirl orbit is always in the direction of impeller rotation. Hence one important conclusion is that this stiffness matrix has an essential destabilizing rotordynamic effect. Of course the rotordynamic consequences of such excitation will depend on the damping matrix as well. In other words this whirl motion will be suppressed if the damping force due to the whirling motion is sufficient. However since K^*_{XY} and K^*_{YX} are proportional to N^2, it follows that if damping increases more slowly with N, then there will always be a speed above which the excitation will exceed the damping. This indicates that hydrodynamic stiffness due to the flow through the rotor and its surroundings can be a possible cause of "rough-running" of pumps.

We now examine the effect of parameter variation on the normalized force matrix. To accomplish this, rotor speeds higher than those shown in Fig. 7 were carried out. A slight increase in the magnitudes of K^*_{ij} was found at rotor speeds of 1200 and 2000 rpm (see [5]). We take this to be a Reynolds number effect. Data has also been obtained with face seal clearances of 0.79 mm and the results are shown in Fig. 8. These findings are qualitatively similar to those in Fig. 7 except that the magnitude of all the components is up to 20 percent larger for the larger clearances. This figure also contains the static pressure force matrix, the results of which will be explained later.

Results for the circular volute (*B*) are shown in Fig. 9. These were surprising in the sense that the skew-symmetric effect was even clearer and that, contrary to Volute *A*, the K^*_{ij} coefficients increased with decreasing flow rate.

In conclusion, no change in the experimental parameters altered the skew-symmetric behavior of the $[K^*]$ matrix. The magnitudes of the K^*_{ij} for different volutes and operating conditions are qualitativey similar.

Combining the volute force results of the previous section along with the hydrodynamic forces matrices of this section

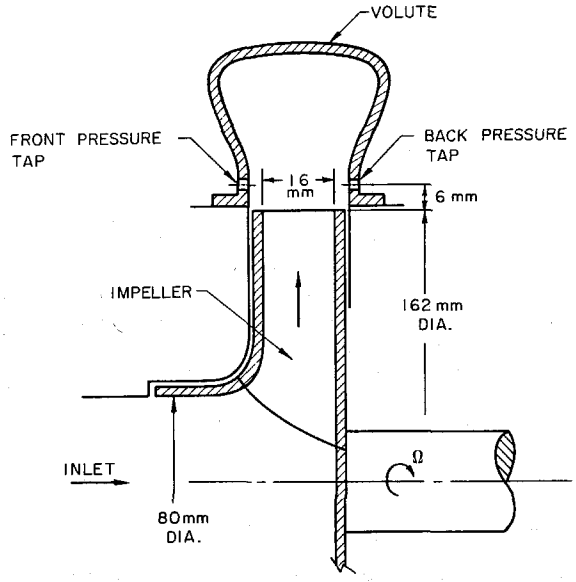

Fig. 11 Schematic showing main dimensions and static measurement points within Volute *A*. There are eight pressure taps more or less equally spaced around the volute circumference on the front and back.

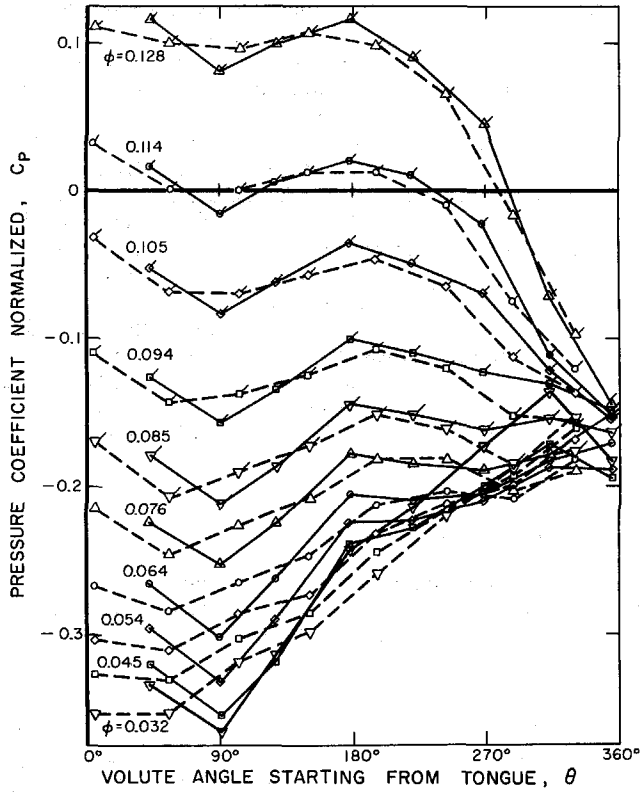

Fig. 12 Pressure coefficients for various flow rates for a rotor speed of 600 rpm. Impeller *X*, Volute *A* and face seal clearances of 0.79 mm. The shaft center position is at the closest point as defined by Fig. 3. Solid lines represent the front pressure taps and dashed lines the back pressure taps of Fig. 11. (Uncertainty in Θ = ±2 deg, in C_p = ±0.007).

gives the geometric position of the impeller within its volute casing such that the total steady-state impeller force is zero. For Volute *A* the locus of these "hydrodynamic centers" exhibits a linear region between the flow coefficients of 0.055 and 0.122 (see reference [5]), which agrees well with the results of Domm and Hergt [7].

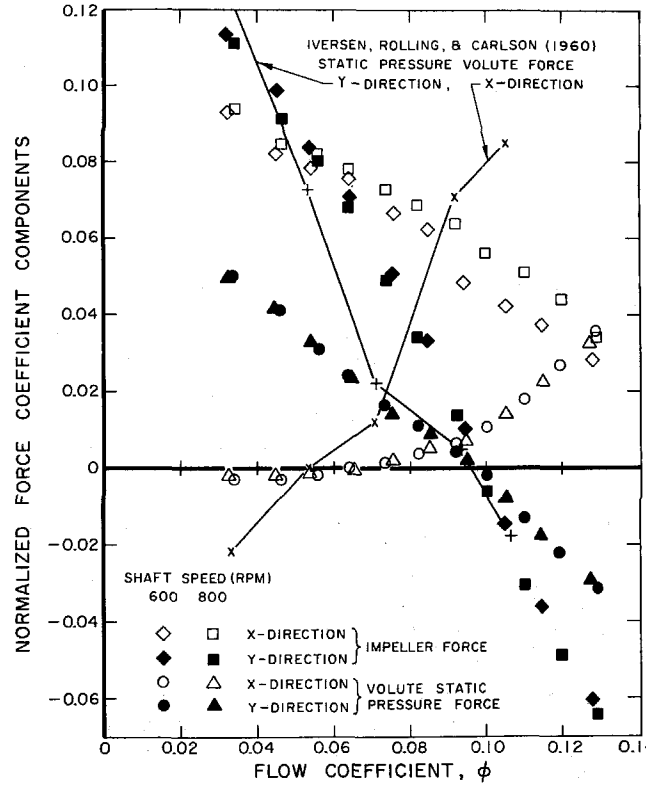

Fig. 13 Normalized impeller forces and static pressure forces of Fig. 12 for rotor speeds of 600 and 800 rpm for Impeller *X*, Volute *A* and face seal clearances of 0.79 mm. The shaft center position is at the closest point as defined by Fig. 3. Comparison is made with Iverson, et al. [10], static pressure volute forces. (Uncertainty in Φ = ±0.0025, in Force = ±0.004).

Auxiliary Experiments

Figure 10 presents the force coefficient data for a number of tests performed with the objective of assessing the source of the large radial forces at shutoff. All of the normalized data presented appeared to be virtually independent of shaft speed indicating that forces are proportional to the square of tip speed. The lack of any appreciable force in the absence of the impeller (No Impeller points) was used *a priori* under "Data Acquisition" to show the forces to be truly due to the presence of the rotor only. Other experiments conducted consisted of testing a solid impeller having the same dimensions of Impeller X and of testing Impeller X with its inlet and/or exit blocked by a sheet of metal. The data for the solid impeller and for Impeller X having its inlet and exit blocked were quite similar for both face seal clearances. We conclude that this force coefficient component (about 0.045) is due to disk friction effects and to the induced pressure gradient acting on the entire exterior surfaces of the impeller. The force coefficient for Impeller X with its exit blocked was almost identical to that of the solid impeller. However, the data with the inlet blocked is significantly higher, probably because the outer recirculation effects are greater. The force data for the flow blocked about three diameters upstream of the impeller is higher still.

Dimensionless force matrix coefficients, K_{ij}^*, for each of the experiments in Fig. 10 were also obtained and reported in [5]. The most significant finding is the absence of "stiffness" when the impeller was removed. This confirms the fact that the stiffness force so measured is due to the presence of the rotor. Results for the solid impeller were found to be four times smaller than those at design conditions indicating the contribution of the disk friction effects for the original im-

peller. All of these force matrices remained the sum of diagonal and skew-symmetric matrices [5].

Static Pressure Measurements in the Volute

It would be interesting to learn more about the origins of the impeller hydrodynamic forces. An obvious dissection of these forces should show momentum flux, static pressure and disk friction components. In this section, we measure and discuss the static pressure component of these forces.

Instrumentation. Static pressure distributions within Volute A were measured by means of the static pressure taps shown in Fig. 11 at four fixed positions of the eccentricity (the positions "closest," "farthest," "right" and "left" shown in Fig. 3) at various flow coefficients. A bank of inverted water manometers was used to measure pressure differences for the 16 taps of Fig. 11. The pressure measurements were referenced to the downstream total pressure as measured by an accurate Heise gage. The pressure distributions were then reduced to dimensionless pressure coefficients, C_p, based on the downstream total pressure and the dynamic head at the impeller tip (see Nomenclature). C_p is then plotted against θ, the angle being measured from the cutwater of the volute. Finally, static pressure forces were calculated from these pressure distributions.

Static Pressure Distributions. Figure 12 presents a typical static pressure distribution at the impeller discharge of Impeller X within Volute A at various flow coefficients. The face seal clearances were 0.79 mm and the rotor speed was 600 rpm. The plots represent results from a test at the closest position as shown in Fig. 3. The form and magnitude of the pressure variations are similar to those measured by Iversen, et al. [10] and to those predicted theoretically by Kurokawa [11]. The most important feature is the static pressure discontinuity that occurs in the neighborhood of the cutwater (compare the values of C_p at $\theta = 0°$ and $\theta = 360°$) particularly at off-design flow coefficients. However, at or close to the design value of 0.092, the static pressure is quite uniform around the volute periphery. Finally, we should emphasize the disagreement between the front pressure taps and the back pressure taps measurements of Fig. 11 particularly at low flow coefficients. This suggests that the flow coming out of the impeller is not symmetrical with respect to the centerline of the volute cross section.

Static Pressure Forces. Figure 13 presents the X and Y components of the static pressure force expressed in the coordinates of Volute A for the closest eccentric position (see Fig. 3) and compares them with the total force components on the impeller measured by the external balance for the same impeller location. Note that the static pressure component is not sufficient in itself to explain the measured total force. This is contrary to the results obtained by Iversen, et al. [10]; they observed significant agreement between these forces. They exhibit the same general trend as ours but are much larger in magnitude; this is perhaps due to the lower specific speed of the pump (0.36 instead of 0.57). We conclude that the nonisotropy of the momentum flux leaving the impeller is an important contributor to the impeller forces.

Static Pressure Force Matrix. Hydrodynamic force matrices, $[KP]$, due to the static pressure force components were also calculated and these are shown in Fig. 8 for a rotor speed of 600 rpm and for face seal clearances of 0.79 mm. It transpires that the components of this matrix represent only about 20 percent of the magnitude of the corresponding total hydrodynamic force matrix components. In addition we have shown earlier that disk friction contributes to about 25 percent of this matrix. We therefore conclude that the nonisotropy of the momentum flux is the primary contributor to the "stiffness" matrix. This fact emphasizes the need for direct measurement of the forces on the impeller rather than estimating the latter by integrating pressure distributions around the base circle of the volute.

Measurements Error

Rotor speeds and pump flow rates were read by digital voltmeters and showed negligible drifts or oscillations. The maximum error for the smallest values of these quantities (except for shutoff) was less than one percent. The net eccentricity has a relative error of 0.4 percent while impeller dimensions were measured to ± 0.2 percent. It was felt the accuracy of the slopes of calibration of the pressure transducers and of the force balance load cell elements was well within a one percent relative error. Finally, the phase angle of the measured forces with respect ot the volute's cutwater are determined to within ± 3 deg due to the uncertainties in exactly locating the data sampling "start" position.

Concluding Remarks

We have presented measurements of the steady-state hydrodynamic forces on a centrifugal pump impeller as a function of position within two geometrically different volutes. These correspond to the forces experienced by the impeller at zero whirl frequency. The hydrodynamic force matrices derived from these measurements exhibit both diagonal and off-diagonal terms of substantial magnitude. The off-diagonal or cross-coupling terms are of the form which would tend to excite a whirl motion in a rotordynamic analysis of the pump. This may be the cause of "rough running" reported in many pumps.

Static pressure measurements in the impeller discharge flow show that the hydrodynamic force on the impeller contains a substantial component due to the nonisotropy of the net momentum flux leaving the impeller. Moreover a similar breakdown of the contributions to the stiffness matrices reveals that the major component of these matrices results from the nonisotropy of the momentum flux.

Fugure plans include direct measurement of the forces due to the momentum flux leaving the impeller and the study of other impeller/volute configurations particularly vaned diffusers. Finally measurement of forces at nonzero whirl frequencies will be initiated in order to obtain a complete picture of the rotordynamic consequences of these hydrodynamic forces.

Acknowledgments

This work was supported by the National Aeronautics and Space Administration under contract No. NAS8-33108 and by a Byron Jackson Fellowship in Fluid Machinery. This support is gratefully acknowledged.

References

1 Agostinelli, A., Nobles, D., and Mockridge, C. R., "An Experimental Investigation of Radial Thrust in Centrifugal Pumps," ASME *Journal of Engineering for Power*, Vol. 82, Apr. 1960, pp. 120–126.

2 Brennen, C. E., Acosta, A. J., and Caughey, T. K., "A Test Program to Measure Fluid Mechanical Whirl-Excitation Forces in Centrifugal Pumps," First Workshop on Rotordynamic Instability Problems in High-Performance Turbomachinery, Texas A&M University, NASA Conference Pub. 2133, 1980, pp. 229–235.

3 Chamieh, D. S., and Acosta, A. J., "Dynamic Forces on a Whirling Centrifugal Rotor," *Proceedings 6th Conference on Fluid Machinery*, Akademiai Kiado, Budapest, Hungary, 1979, pp. 210–219.

4 Chamieh, D. S., "Calculation of the Stiffness Matrix of an Impeller Eccentrically Located Within a Volute," Cavitation and Polyphase Flow Forum, Joint ASME/ASCE Conference, Boulder, CO, 1981, pp. 51–53.

5 Chamieh, D. S., "Forces on a Whirling Centrifugal Pump-Impeller," PhD Thesis, Division of Engineering and Applied Sciences, California Institute of Technology, Pasadena, CA, 1983.

6 Colding-Jorgensen, J., "The Effect of Fluid Forces on Rotor Stability of

Centrifugal Compressors and Pumps," PhD Thesis, Department of Machine Design, Technical University of Denmark, 1979.

7 Domm, H., and Hergt, P., "Radial Forces on Impeller of Volute Casing Pumps," Flow Research on Blading," Dzung, L. S., ed., Elsevier Publishing Co., The Netherlands, 1970, pp. 305–321.

8 Ek, M. C., "Solution of the Subsynchronous Whirl Problem in the High Pressure Hydrogen Turbomachinery of the Space Shuttle Main Engine," Paper No. 78-1002, AIAA/SAE 14th Joint Propulsion Conf., Las Vegas, NV, July 25–28, 1978.

9 Hergt, P., and Krieger, P., "Radial Forces in Centrifugal Pumps With Guide Vanes," Advance Class Boiler Feed Pumps," *Proceedings, Institution of Mechanical Engineers*, Vol. 184, Pt 3N, 1969–1970, pp. 101–107.

10 Iversen, H. W., Rolling, R. E., and Carlson, J. J., "Volute Pressure Distribution, Radial Force on the Impeller and Volute Mixing Losses of a Radial Flow Centrifugal Pump," ASME *Journal of Engineering for Power*, Vol. 82, Apr. 1960, pp. 136–144.

11 Kurokawa, J., "Theoretical Determinations of the Flow Characteristics in Volutes," IAHR/AIRH Symposium, Tokyo, Japan, 1980, pp. 623–634.

12 Ohashi, H., Shoji, H., Yanagisawa, S., and Tomita, K., "Experimental Study of Fluid Forces on Whirling Centrifugal Impeller in Vaneless Diffuser," Symp. Fluid/Structures Interactions in Turbomachinery, Thompson, W. E., ed., ASME Winter Annual Meeting, 1981, pp. 57–62.

13 Pollman, E., Schwerdtfeger, H., and Termuehlen, H., "Flow Excited Vibrations in High Pressure Turbines (Steam Whirl)," ASME *Journal of Engineering for Power*, Vol. 100, Apr. 1978, pp. 219–228.

14 Stepanoff, A. J., *Centrifugal and Axial Flow Pumps*, 2nd ed., Wiley, New York, 1957.

15 Thompson, W. E., "Fluid Dynamic Excitation of Centrifugal Compressor Rotor Vibrations," ASME JOURNAL OF FLUIDS ENGINEERING, Vol. 100, Mar. 1978, pp. 73–78.

DISCUSSION

H. Ohashi[2]

As one who has the same interest in the hydrodynamic forces of whirling centrifugal impellers, I would like to express my respect for carrying out such delicate and complex experiments successfully. Following are a few comments on your result.

1 Despite a remarkable difference in the average volute forces F_0 of Volute A and B, the difference in the stiffness matrices of both volutes is surprisingly small. This may imply that stiffness matrices are insensitive to the configuration of volute casing. It is, however, still unknown how stiffness is affected by impeller geometries.

The result for centrifugal impellers in vaneless diffuser obtained by our test facility [16] showed a smaller diagonal term (about one quarter of equation (4)) and cross-coupling term which was destabilizing at lower flow rate and stabilizing around design flow rate.

Therefore, the stiffness matrices can be quite different from one impeller to another and the result approximately presented by equation (4) seems applicable to a specific impeller.

2 Since the hydrodynamic stiffness of impeller vanes and shrouds are different in nature, the fraction of outlet width b_2 to total width w_2 is an important parameter. Please give the value of the test Impeller X.

3 At lower flow rate close to shutoff, the flow in the impeller becomes quite turbulent and the fluid force fluctuates violently. Have you experienced any measurement problems associated with this phenomena?

Additional Reference

16 Ohashi, H., Shoji, H., and Kato, C., "Experimental Study of Fluid Forces on Whirling Centrifugal Impeller (1st Report; Impeller in Vaneless Diffuser)," Trans. JSME, Vol. 51, No. 467, July 1985, pp. 2373–2381 (in Japanese) or NASA CP 2338, 1985, pp. 109–122.

[2]Mechanical Engineering, University of Tokyo, Bunkyo-Ku, Tokyo 113, Japan.

Authors' Closure

The authors wish to thank Professor Ohashi for his continuing interest in this paper in particular, and this research field in general. The work presented herein was concluded in late 1982 and has since been validated and extended at the Caltech Rotor Force Test Facility to inlcude the full dynamic effect of whirl [17, 18]. Currently additional research was also initiated to study the effects of cavitation inception and net positive suction head on the magnitudes of the stiffness matrix coefficients [19]. While we agree that the similarities between the stiffness matrices of Volutes A and B are relatively striking, additional experiments by Jery, et al. [17] for 7 different volutes/diffusers and 2 different impellers of about the same specific speed seem to validate that fact. The stiffness matrices Professor Ohashi obtained in his very valuable study are much lower than those presented here probably because of the large collector case used in his experiment. An impeller discharging in an infinite medium should have no stiffness coefficients.

The width of the impeller discharge including the shrouds is 26 mm. The internal width of the discharge is 16 mm as shown in Fig. 11. We believe that the latter dimension is the important one.

No wild fluctuation in forces were observed at shutoff for the steady-state measurements presented in this paper. In a communication with B. Jery [17, 18], it also seems that their experimental results were quite consistent and repeatable.

Additional References

17 Jery, B., Brennen, C. E., Caughey, T. K., and Acosta, A. J., "Forces on Centrifugal Pump Impellers," *Proceedings of the 2nd International Pump Symposium*, Houston, TX, April 30–May 2, 1985, pp. 21–32.

18 Jery, B., Acosta, A. J., Brennen, C. E., and Caughey, T. K., "Hydrodynamic Impeller Stiffness, Damping and Inertia in the Rotordynamics of Centrifugal Flow Pumps," *Workshop on Rotordynamic Instability Problems in High-Performance Turbomachinery*, Texas A&M University, NASA Conference Publication 2338, 1984, pp. 137–160.

19 Franz, R., Acosta, A. J., Brennen, C. E., and Caughey, T. K., "Effects of Cavitation on the Radial Forces in a Centrifugal Pump," to be published, Oral presentation by C. E. Brennen at the 2nd Joint ASCE/ASME Mechanics Conference, University of New Mexico, Albuquerque, June 23–26, 1985.